Z. WANG[1]
S. FAN[2],✉

Magneto-optical defects in two-dimensional photonic crystals

[1]Department of Applied Physics, Stanford University, Stanford, CA 94305-4090, USA
[2]Department of Electrical Engineering, Stanford University, Stanford, CA 94305-8085, USA

ABSTRACT We analyze the properties of magneto-optical defect states in two-dimensional photonic crystals. With out-of-plane magnetization, the magneto-optical coupling splits doubly-degenerate TE states into two counter-rotating modes at different frequencies. The strength of magneto-optical coupling strongly depends on the spatial overlap of the cavity domain structures and the cross product of the modal fields. The transport property of the resultant nonreciprocal states is demonstrated in a junction circulator structure with a magneto-optical cavity coupled to three waveguides. By a proper matching of the magneto-optical frequency splitting with the cavity decay rate into the waveguide, ideal three-port circulator characteristics with complete isolation and transmission can be achieved, with an operational bandwidth proportional to the magneto-optical constant. The proposed optical circulator in a bismuth-iron-garnet/air photonic crystal is demonstrated with finite-difference time-domain calculations and is compared to an alternative implementation of silicon/air crystal infiltrated with a single bismuth-iron-garnet domain.

PACS 42.70.Qs; 42.82.Et; 85.70.Sq

1 Introduction

The continuing dramatic increase in bandwidth demand in today's data-communication networks has triggered the need of higher component density to sustain the growth of broadband optical networks. Among the intensive research efforts on miniaturizing optical components down to chip level, integrated non-reciprocal optical devices, such as optical isolators and circulators, have attracted much attention. An ideal nonreciprocal device allows signals to be transmitted unidirectionally through an optical circuit, without attenuation and degradation. Besides the typical applications in eliminating the detrimental reflections to laser sources as their bulk counter-part [1], integrated non-reciprocal devices also simplify the design of large-scale optical circuits by suppressing multi-path reflections between components, and thereby im-proving tolerance with respect to fabrication imperfections and environmental fluctuations.

A common approach to obtain non-reciprocity at optical wavelength is based on a linear magneto-optical effect, known as gyrotropy. It has been used in most commercially-available bulk optical isolator or circulator structures, where large isolation and minimal insertion loss can be simultaneously achieved. The dimension of such devices, however, tends to be very large at a length scale on the order of millimeters. The strength of gyrotropy in existing magneto-optical material, measured by the Voigt parameter, is at most 10^{-2} and typically less than 10^{-3}. Consequently the signal interaction length needs to be at least hundreds of wavelengths. This requirement for a long interaction length also applies to many integrated magneto-optical devices including waveguide isolators with nonreciprocal phase shift [2–4]. In these devices, while the lateral dimensions have been reduced to several microns, the length remains comparable to bulk devices.

To reduce the length of the devices, magneto-optical resonators have been developed to trade the operational bandwidth for shorter optical path. Already demonstrated experimentally, enhanced Faraday rotation in one-dimensional photonic crystal defect systems can significantly shorten the total device length necessary for a $45°$ polarization rotation by one order of magnitude [5, 6]. The application of such scheme in today's on-chip optical circuits, however, is fundamentally limited by the problem of weak light confinement in the transversal dimension, which results in large lateral component sizes, and the inconvenient co-linear magnetic biasing. In this context, two-dimensional photonic crystals are promising candidates for the advancement of sub-wavelength non-reciprocal optical devices, thanks to its strong in-plane field confinement from the photonic band gap and the compatibility with planar on-chip circuits. The strongly localized defect states in these systems provide new degrees of freedom to control the transfer function of the devices through patterned domain structures.

In this paper, we present an analysis of nonreciprocal magneto-optical resonators in two-dimensional photonic crystals. We discuss the use of such resonators in high-performance and large-bandwidth planar optical circulator structures that are extremely compact. In addition, we will show that the transport properties of these devices are strongly

✉ Fax: +1-650-725-2533, E-mail: shanhui@stanford.edu

influenced by domain structures. Thus by rewriting the domain, one can readily reprogram the optical circuits.

The paper is organized as follows: In Sect. 2, we theoretically describe the modal structures of a magneto-optical defect in a photonic crystal using a perturbation approach. We show that such defect can support counter-rotating modes that are singly degenerate. The frequency splitting between these modes, which is proportional to the magneto-optical coupling strength, strongly depends on the overlap between the modal cross-product and the magnetic domain structure. In Sect. 3, we then present a systematic approach for optimizing the domain structure to magneto-optical coupling strength. In Sect. 4, we show that the existence of such singly-degenerate counter-rotating modes can be used to design a circulator, and we introduce a temporal coupled-mode theory for such circulators. Finally, in Sect. 5, the theoretical approaches in Sects. 2–4 are validated with first-principle finite-difference time-domain simulations on photonic crystal structures.

2   Magneto-optical coupling of defect states

Before we discuss magneto-optical defect structures in photonic crystals, let's briefly review some of the basic properties of magneto-optical materials. At optical wavelengths, the gyrotropy of a magneto-optical material is characterized by a dielectric tensor:

$$\overset{\leftrightarrow}{\varepsilon} = \begin{pmatrix} \varepsilon_\perp & i\varepsilon_a & 0 \\ -i\varepsilon_a & \varepsilon_\perp & 0 \\ 0 & 0 & \varepsilon_\parallel \end{pmatrix}, \tag{1}$$

when the magnetization is along the z direction. Here, for simplicity, we ignore the absorption and assume $\varepsilon_\perp$, $\varepsilon_\parallel$ and ε_a to be real. The ε_a in the off-diagonal elements has its sign dictated by the direction of magnetization. The strength of magneto-optical effects is measured by the Voigt parameter $Q_M = \varepsilon_a/\varepsilon_\perp$.

To theoretically describe the modes in a magneto-optical defect structure in a photonic crystal, we use a Hamiltonian formalism [7], where the resonator mode $|\psi\rangle = \begin{bmatrix} \vec{E} \\ \vec{H} \end{bmatrix}$ at a frequency ω is the solution of the eigenvalue equation

$$\Theta |\psi\rangle = \omega |\psi\rangle, \tag{2}$$

with

$$\Theta = \begin{bmatrix} 0 & i\overset{\leftrightarrow}{\varepsilon}^{-1}\vec{\nabla}\times \\ -i\mu_0^{-1}\vec{\nabla}\times & 0 \end{bmatrix} \tag{3}$$

as defined by Maxwell's equations.

This eigenvalue equation can be solved numerically. Here, however, to exhibit the general features of modal structures in a magneto-optical resonator, we exploit the fact that the Voigt parameter is typical less than 10^{-3} and use a perturbative approach where the Hamiltonian is split into a non-magneto part Θ_0 and a gyrotropic perturbation $\mathbf{V}$ as $\Theta = \Theta_0 + \mathbf{V}$, where

$$\Theta_0 = \begin{bmatrix} 0 & i\varepsilon_\perp^{-1}\vec{\nabla}\times \\ -i\mu_0^{-1}\vec{\nabla}\times & 0 \end{bmatrix}$$

$$\mathbf{V} = \begin{bmatrix} 0 & i(\overset{\leftrightarrow}{\varepsilon}^{-1} - I\varepsilon_\perp^{-1})\vec{\nabla}\times \\ 0 & 0 \end{bmatrix}. \tag{4}$$

The effects of gyrotropy are entirely encapsulated by V, which induces magneto-optical coupling between the eigenmodes of the non-magnetic photonic crystal described by Θ_0.

For concreteness, we consider the simple case of a system supporting two nearly-degenerate defect states, where the effect of magneto-optical coupling is particularly prominent. The structure shown in Fig. 1a consists of a two-dimensional photonic crystal with a triangular lattice of air holes in Bismuth Iron Garnet (BIG) with $\varepsilon_\perp = 6.25$ (Fig. 1a). The air holes have a radius of $0.35a$, where a is the lattice constant. The corresponding nonmagnetic photonic crystal (described by Θ_0) exhibits a large TE bandgap in the frequency range of 0.302 to 0.403 c/a. Reducing the radius r of a single air hole creates a pair of degenerate dipole defect modes into the bandgap (Fig. 1b). A cavity with $r = 0$ supports modes at a mid-gap frequency of 0.346 c/a. These two modes can be categorized as an even mode $|e\rangle$ (Fig. 2a) and an odd mode $|o\rangle$ (Fig. 2b) with respect to the y-direction mirror symmetry plane of the crystal. Equivalently, the two eigenmodes can be also chosen as a pair of rotating states $(|e\rangle \pm i|o\rangle)/\sqrt{2}$ [8]. Since Θ_0 by itself possesses time-reversal symmetry, these two rotating modes, which transform into each other with a time-reversal operation, necessarily have the same frequency.
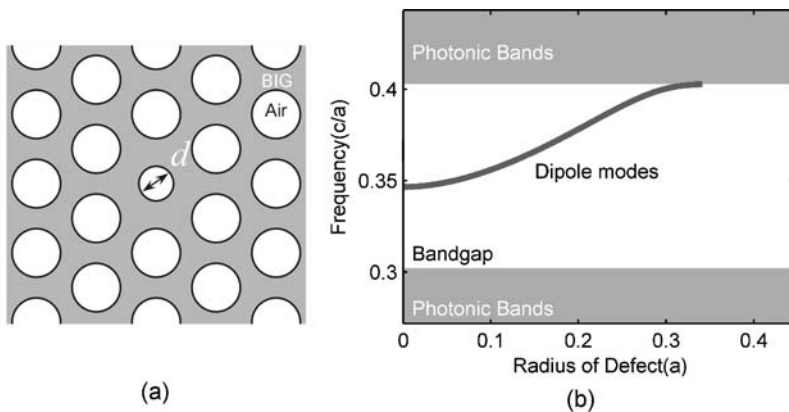

FIGURE 1 **a** A defect structure in a photonic crystal. The crystal consists of a triangular lattice of air holes with a radius of $0.35a$, introduced in a dielectric of $\varepsilon = 6.25$. The defect is created by reducing the radius of a single air hole. **b** The frequency of the defect modes as a function of the radius of the center air hole in the defect region for the two-dimensional bismuth-iron-garnet photonic crystal. The calculation is performed using a plane-wave expansion method [20]
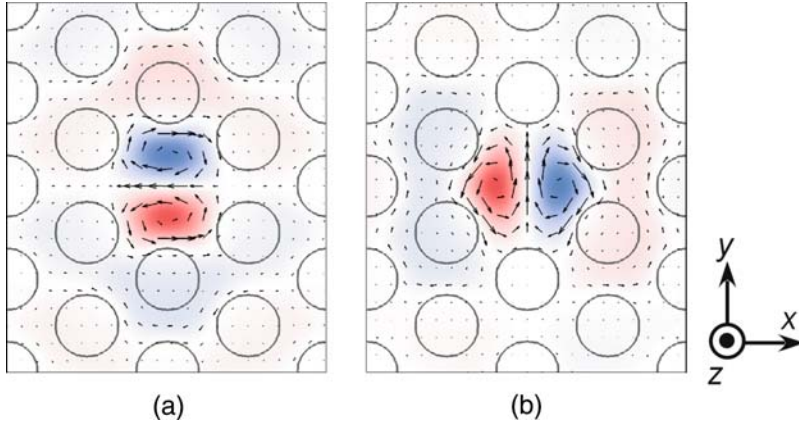
FIGURE 2   The colored images represent the Hz field distribution of the two doubly-degenerate dipole modes in the BIG photonic crystal cavity as shown in Fig. 1. The blue and red colors represent large positive and negative values. The vector plots represent the E fields

The effect of gyrotrophy, described by the operator V, is to introduce magneto-optical coupling between the eigenmodes of Θ_0. With the basis of the eigenmodes of Θ_0, the Hamiltonian Θ can be rewritten as [7]

$$\Theta_0 = \sum_\alpha \omega_\alpha |\psi_\alpha\rangle\langle\psi_\alpha|, \qquad \mathbf{V} = \sum_{\alpha,\beta} \mathbf{V}_{\alpha\beta} |\psi_\alpha\rangle\langle\psi_\beta|. \qquad (5)$$

To the first order of ε_a, the coupling strength between any two modes α and β can be derived as:

$$\mathbf{V}_{\alpha\beta} = \frac{i}{2} \frac{\sqrt{\omega_\alpha\omega_\beta} \int \varepsilon_a \hat{\mathbf{z}} \cdot \left(\vec{E}^*_\alpha \times \vec{E}_\beta\right) \mathrm{d}V}{\sqrt{\int \varepsilon_\perp |\vec{E}_\alpha|^2 \mathrm{d}V \int \varepsilon_\perp |\vec{E}_\beta|^2 \mathrm{d}V}}, \qquad (6)$$

where the sign of ε_a is determined by the direction of the magnetization vector, and $\vec{E}_\alpha$ is the electrical field for the unperturbed mode $|\psi_\alpha\rangle$. Thus the magneto-optical coupling is closely related to the spatial arrangement of the magnetic domain as well as the vectorial field distribution of the defect states.

When we choose the standing-wave modes with real-valued electromagnetic fields as the eigenmode basis, the coupling constant between them is purely imaginary. Therefore, for the structure as shown in Fig. 2, in the subspace of $|e\rangle$ and $|o\rangle$, when $\omega_e = \omega_o$, the Hamiltonian of the system is

$$\Theta = \begin{pmatrix} \omega_e & \mathbf{V}_{eo} \\ -\mathbf{V}_{eo} & \omega_e \end{pmatrix} \qquad (7)$$

when magneto-optical materials are present in the cavity. The eigenstates for the Hamiltonian in Eq. (7) take the rotating wave form $|e\rangle \pm i |o\rangle$, with a frequency splitting of $2|\mathbf{V}_{eo}|$. Since the two counter rotating modes are related by a time-reversal operation, the frequency splitting between them clearly indicates the breaking of time-reversal symmetry and reciprocity. Also, importantly, even in the case where ω_e deviates from ω_o, for example due to fabrication related disorders that break the three-fold rotational symmetry, as long as the magneto-optical coupling is sufficiently strong, i.e.$|\mathbf{V}_{eo}| \gg |\omega_e - \omega_o|$, $|e\rangle \pm i |o\rangle$ remain the eigenstates of the system. Thus, in the limit of strong magneto-optical coupling, such modes assume a general waveform of circular hybridization independent of small structural disorders that would almost always occur in practical devices. A device

whose operation relies upon the presence of such rotating states will therefore be robust against small disorders.

3   Optimization of the domain structure

Given the importance of obtaining large magneto-coupling strength $|\mathbf{V}_{eo}|$, we now proceed to maximize the spatial overlap between domain structure and the modal fields in Eq. (6). Due to the vectorial nature of defect states in photonic crystals, the cross product between the electric fields of the even mode $|e\rangle$ and the odd mode $|o\rangle$ changes sign rapidly in the cavity, as shown in Fig. 3a. Thus, if the cavity consists of a single magnetic domain, the coupling strength diminishes. ($|\mathbf{V}_{eo}|$ is numerically evaluated as $1.2 \times 10^{-3} |\varepsilon_a| \omega_{oe}$ in this
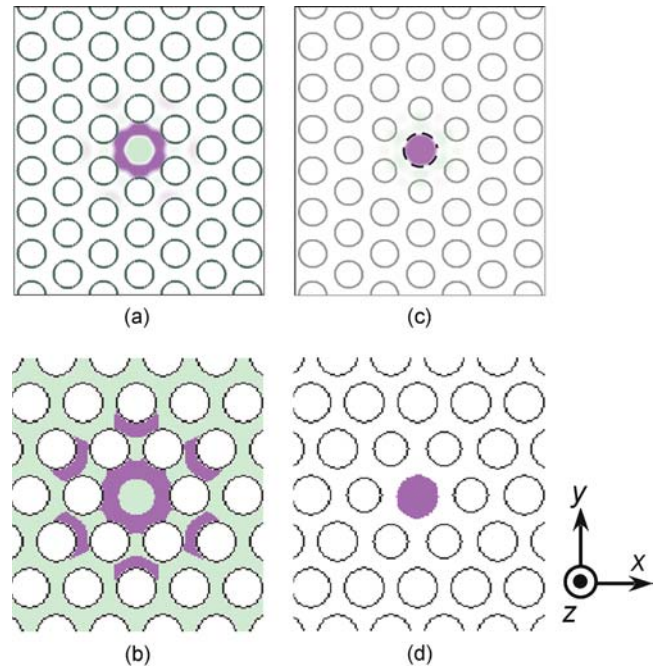

FIGURE 3   a The cross-product between the E-fields of the two modes shown in Fig. 2. b The corresponding domain pattern that maximizes the magneto-optical coupling constant. c The spatial distribution of the modal cross-product of the dipole modes in an infiltrated BIG cavity in a silicon crystal. The Black dashed circle represents the position of the BIG rod. d The corresponding optimized domain pattern using only single domain. In all these plots, the cyan and magenta colors represent large positive and negative values

case.) On the other hand, the magneto-optical coupling can be maximized by inverting the domain structures according to the signs of the modal cross product. The appropriate domain structure that maximally couples the two modes $|e\rangle$ and $|o\rangle$ is shown in Fig. 3b, where the minimum feature size is about 150 nm for 1550 nm operational wavelength. (We note that domain structures with dimensions on the order of 18 nm have been fabricated experimentally [9].) For a constant $|\varepsilon_a|$ in the entire cavity region, the maximum $|\mathbf{V}_{eo}|$ obtained with such domain structure is $0.0695\,|\varepsilon_a|\,\omega_{oe}$, nearly 50 times greater than the case of a uniform domain.

Alternatively, since the cross product of the modal field is well localized in the defect due to the strong field confinement from the photonic band gap, we can employ a simpler domain configuration, while still maintaining a moderately strong magneto-coupling. As an example, consider a silicon/air cavity similar to Fig. 1b with a single BIG domain covering the center part of the cavity. Because of the index difference between silicon and BIG, the radius of the nodal circle of the modal cross product depends on the size of the BIG rod. Such dependence affects the overlap and results in an optimal radius $r = 0.4a$ where $|\mathbf{V}_{eo}|$ is maximized, as shown in Fig. 4a. At this radius, the magneto-optical material completely filled the center region with a constant sign on the modal cross product shown in Fig. 3c. For the optimized structure shown in Fig. 3d, we show the magneto optical coupling constant as a function of the off-diagonal part in the dielec-
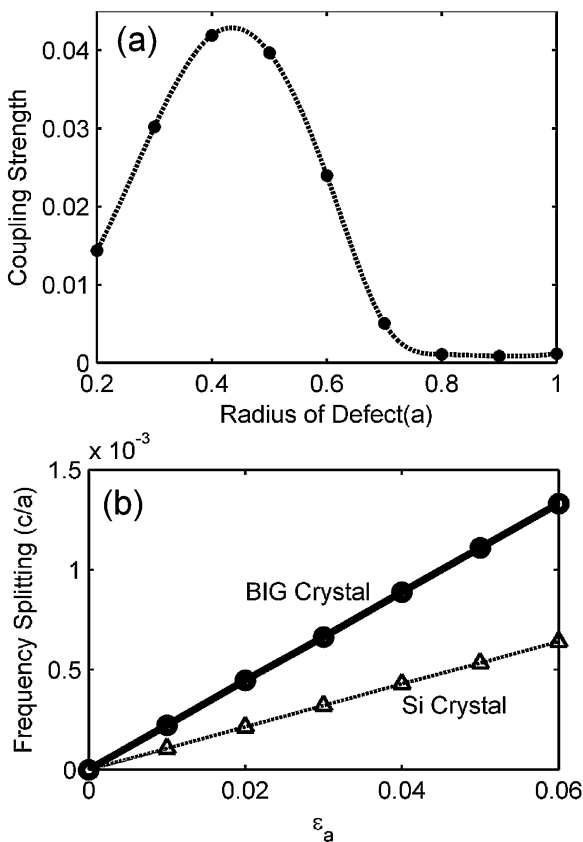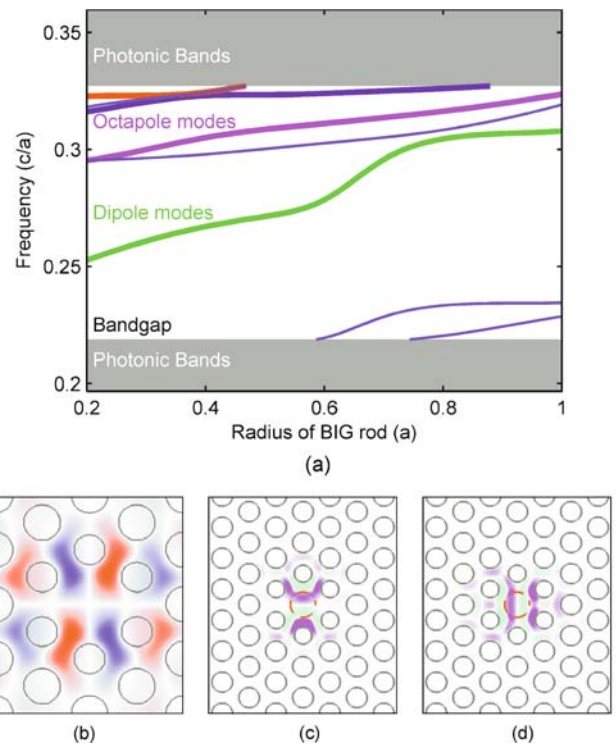

(a)

(b) (c) (d)

FIGURE 5 a The frequency of the defect modes as a function of the radius of the center BIG rod in the defect region for the two-dimensional silicon photonic crystal. **b** An octapole mode in the infiltrated silicon cavity with $r_{BIG} = 0.4a$. **c** The modal cross product of this octapole mode with the even mode in Fig. 2a. **d** The modal cross product of the octapole mode with the odd mode in Fig. 2b. The red dashed circles represent the position of the BIG rods. The radius of the six holes next to the center defect is reduced to $0.3a$ to push the dipole modes to the center of the gap

FIGURE 4   a The magneto-coupling strength in an infiltrated silicon photonic crystal cavity as a function of the radius of the BIG rod. **b** The magneto-optical splitting between the dipole modes as a function of ε_a for the cavity in BIG crystal and the infiltrated silicon cavity with $r_{BIG} = 0.4a$

tric tensor, calculated by the finite-difference time-domain (FDTD) method (Fig. 4b). When compared with the pure BIG crystal with inverted domains, the Si/BIG hybrid cavity produces a slightly smaller coupling strength. Nevertheless, the simplified domain structure should facilitate experimental set up to achieve fully saturated magnetization under external magnetic biasing.

In the Si/BIG hybrid cavity structure, in addition to the dipole modes, there exist other modes inside the photonic band gap (Fig. 5a), including, for example, the octapole mode as shown in Fig. 5b. In principle, the presence of magneto-optical materials can create coupling between the dipole modes and these modes with other symmetries. The required domain structure for such a coupling can be inferred from the modal cross-product as shown in Fig. 5c and d. These modal cross-products feature a nodal plane at the center and has an odd mirror symmetry. Thus, with our choice of domain structures that has the full even symmetry of the structure, the magneto-optical couplings between modes from different irreducible representations are forbidden. In addition, as can be seen from Eq. (7), the effects of coupling between any two modes are weak if the frequency difference between the modes is large enough. Therefore, in the following analysis, we will be focusing primarily on the dipole modes while ignoring all the other modes in the system.

4   Temporal coupled-mode theory of optical circulators

As an application of the rotating states in the magneto-optical resonators, as discussed above, we now construct an optical circulator by using these rotating modes to create direction-dependent constructive or destructive interference. The structure is schematically shown in Fig. 6a, with three branches of waveguides (ports) evanescently coupled to a resonant cavity at the center. For simplicity, we assume the structure have 120-degree rotational symmetry. Ideally, at the signal frequency the device shall allow complete transmission from ports 1 to 2, 2 to 3, and 3 to 1, while prohibiting transmission in the reversed directions. This transport characteristic can be accomplished with an appropriate choice of frequency splitting with respect to the decay rate of the resonance.

The system as shown in Fig. 6a can be described by the following temporal coupled mode theory equations [10–12]:
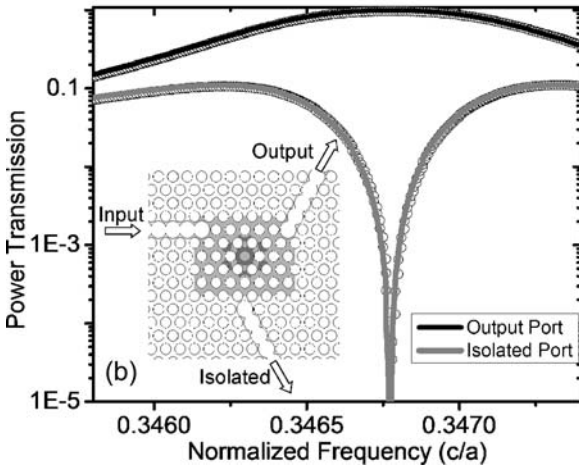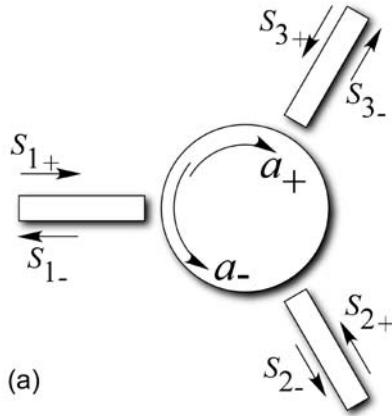

(a)

(b)

FIGURE 6 **a** Schematics of a three-port Y-junction circulator. The straight arrows indicate the incoming and outgoing waves. The curved arrows represent the two counter-rotating modes in the resonator. **b** Transmission spectra at the output and isolated ports of a three-port junction circulator shown in the inset. The circulator is constructed as a point defect coupled to three waveguides. Circles correspond to air holes in Bismuth Iron Garnet. The light and dark gray areas represent the magnetic domains with opposite out-of-plane magnetization direction. The finite-difference time-domain spectra (*dots*) agree well with the coupled-mode theory analysis (*solid curves*)

$$\frac{\mathrm{d}}{\mathrm{d}t}\begin{pmatrix} a_+ \\ a_- \end{pmatrix} = \begin{pmatrix} i\omega_+ - \gamma_+ & 0 \\ 0 & i\omega_- - \gamma_- \end{pmatrix}\begin{pmatrix} a_+ \\ a_- \end{pmatrix}$$
$$+ \mathbf{K}^{\mathrm{T}}\begin{pmatrix} S_{1+} \\ S_{2+} \\ S_{3+} \end{pmatrix}, \tag{8}$$

$$\begin{pmatrix} S_{1-} \\ S_{2-} \\ S_{3-} \end{pmatrix} = \begin{pmatrix} -1 & 0 & 0 \\ 0 & -1 & 0 \\ 0 & 0 & -1 \end{pmatrix}\begin{pmatrix} S_{1+} \\ S_{2+} \\ S_{3+} \end{pmatrix} + \mathbf{D}\begin{pmatrix} a_+ \\ a_- \end{pmatrix}. \tag{9}$$

$a_{+(-)}$ is the normalized field amplitude of the counter-clockwise (clockwise) rotating mode. These modes resonate at frequencies $\omega_{+(-)}$ and decay at rates $\gamma_{+(-)}$. $S_{i+(-)}$ is the normalized amplitude of the incoming (outgoing) wave at port i. The 3×2 matrices, $\mathbf{K}$ and $\mathbf{D}$, represents the coupling between the resonances and the waves at the ports. Unique in magneto-optical system under DC magnetic bias, the full time-reversal operation should include the reversal of external DC magnetic field [13]. Thus, a full time-reversal operation flips the rotation directions of the cavity modes, and hence transform $\mathbf{K}$ to $\mathbf{K}^*$. Taking into account energy conservation and time-reversal properties of the structure, we can arrive at the following relations:

$$\mathbf{D}^+\mathbf{D} = 2\begin{pmatrix} \gamma_+ & 0 \\ 0 & \gamma_- \end{pmatrix}, \tag{10}$$

$$\mathbf{K}^* = \mathbf{D}, \tag{11}$$

$$\begin{pmatrix} -1 & 0 & 0 \\ 0 & -1 & 0 \\ 0 & 0 & -1 \end{pmatrix}\mathbf{D}^* = -\mathbf{D} \tag{12}$$

These conditions, in combination of the 120-degree rotational symmetry of the structure, leads to:

$$\mathbf{K}^* = \mathbf{D} = \begin{pmatrix} \sqrt{2\gamma_+/3} & \sqrt{2\gamma_-/3} \\ e^{-i2\pi/3}\sqrt{2\gamma_+/3} & e^{i2\pi/3}\sqrt{2\gamma_-/3} \\ e^{-i4\pi/3}\sqrt{2\gamma_+/3} & e^{i4\pi/3}\sqrt{2\gamma_-/3} \end{pmatrix}. \tag{13}$$

In this derivation, we also assume that the main non-reciprocal effect of the magneto-optical materials is to introduce the frequency split between the counter rotating modes, while the coupling between these modes with the waveguides contain no non-reciprocal phase shift.

When wave at frequency ω is incident from port 1, the power transmission coefficients at ports 2 and 3 are solved from Eqs. (8)–(13) as:

$$T_{1\to2} = \left| \frac{2}{3}\left(\frac{\exp(i4\pi/3)}{1 + i(\omega - \omega_+)/\gamma_+} + \frac{\exp(i2\pi/3)}{1 + i(\omega - \omega_-)/\gamma_-} \right) \right|^2$$

$$T_{1\to3} = \left| \frac{2}{3}\left(\frac{\exp(i2\pi/3)}{1 + i(\omega - \omega_+)/\gamma_+} + \frac{\exp(i4\pi/3)}{1 + i(\omega - \omega_-)/\gamma_-} \right) \right|^2, \tag{14}$$

The ideal circulator response with $T_{1\to3} = 1$ and $T_{1\to2} = 0$ can be obtained at an operational frequency ω_0, when the
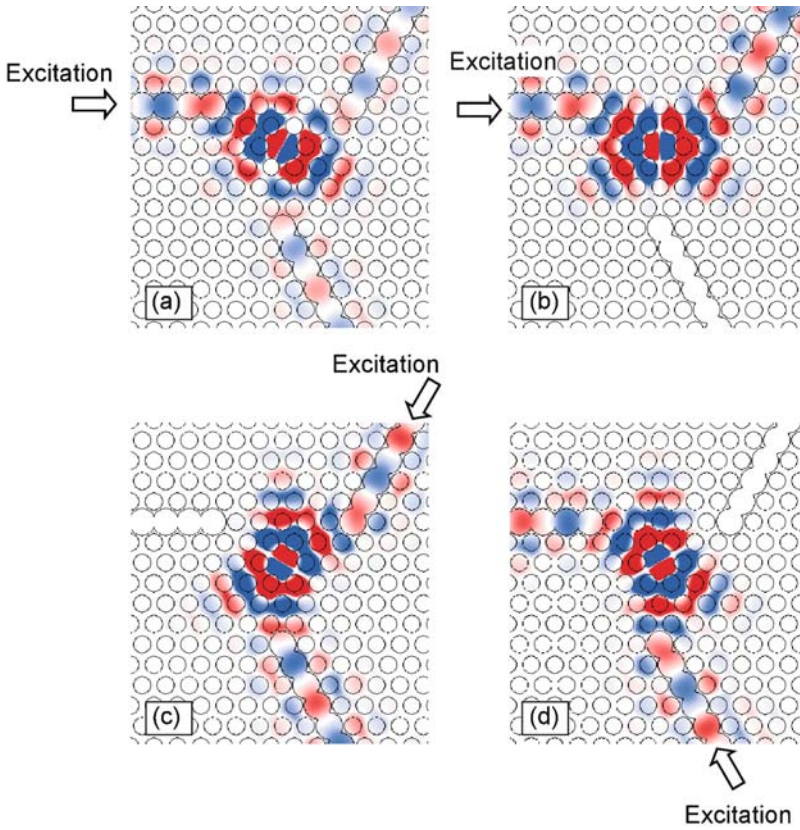
FIGURE 7 Out-of-plane H field patterns of the three-port junction circulator shown in Fig. 3 when excited at $\omega = 0.3468$ (c/a). The red and blue colors represent large positive and negative values. **a** Non-magneto-optical cavity ($\varepsilon_a = 0$) excited at the input port; **b** a magneto-optical cavity with $\varepsilon_a = 0.02463$, excited at the input port; the identical magneto-optical cavity is also seen as excited at the output port in **c** and at the isolated port in **d**

resonant frequencies are chosen to satisfy the following conditions[1]:

$$\omega_+ = \omega_0 + \gamma_+/\sqrt{3} \quad \text{and} \quad \omega_- = \omega_0 - \gamma_-/\sqrt{3} \qquad (15)$$

In such a case, ports 2 and 3 function as the isolated and the output ports, respectively. (The roles of ports 2 and 3 are switched with $\omega_+ < \omega_-$.) From Eqs. (14) and (15), the transfer function from the input port to the output port takes a symmetric form with respect to ω_0 when $\gamma_+ \approx \gamma_-$. In this case, the structure possesses maximum bandwidth for given magneto-optical splitting $|\omega_+ - \omega_-|$. The bandwidth for 30-dB isolation can be determined to be $0.0548 |\omega_+ - \omega_-|/\pi$ in the vicinity of ω_0 using Eq. (14). Also, by rotational symmetry of the structure, we have $T_{1\rightarrow 2} = T_{2\rightarrow 3} = T_{3\rightarrow 1} = 0$, and $T_{2\rightarrow 1} = T_{3\rightarrow 2} = T_{1\rightarrow 3} = 1$. Thus, transmission at frequency ω_0 is allowed only along the clockwise direction. Such a structure therefore behaves as an ideal circulator.

5   Numerical demonstration

To validate the theoretical analysis, we compare the analytical coupled-mode theory conclusion with first-principles FDTD calculations with a gyrotropic material model [14]. Using the BIG resonator we discussed in Sect. 4, a three-port Y-junction circulator is created by coupling three waveguides to the cavity (Fig. 6b inset). Each waveguide is

constructed by enlarging the radius of a row of air holes to $0.55a$. Such waveguides are single-moded at the mid-gap frequencies. These waveguides are spatially arranged to preserve the three-fold rotational symmetry. This configuration also provides excellent control over the coupling between the cavity modes and the waveguides, as the quality factor increases monotonically with distance between the waveguide and the cavity [15]. To reduce computational costs we only include the magneto-optical domain in the vicinity of the cavity region. Filling the remaining computational cell with a single-magnetic domain shows no noticeable differences in the transport properties, since the fields are strongly localized in the cavity region and the waveguides are reciprocal due to the symmetric domain structure [16]. Thin bands of nonmagnetic region have been placed at the air-dielectric interface around the air holes to prevent numerical instability in FDTD simulations. The presence of these bands slightly reduced the maximum magneto-splitting achievable in time-domain calculation for given value of ε_a. (Since the use of a rectangular grid for triangular lattices itself breaks 3-fold rotational symmetry, we have also compensated the numerical dispersion by small modification in the cavity region.)

In the transmission calculation with FDTD method, we choose $\varepsilon_a = 0.02463$. With the choice, the two rotating modes have frequencies 0.3465 (c/a) and 0.3471 (c/a), and quality factors 364 and 367, satisfying the conditions in Eq. (14). The FDTD calculations indeed demonstrate nearly ideal three-port circulator characteristics and agree nicely with the coupled-mode theory (Fig. 6b). The numerical simulations thus confirm the validity of temporal coupled mode theory

---

[1]A similar condition has been derived for a microwave ferrite circulator in D.M. Pozar, *Microwave Engineering* (John Wiley, New York, 1998). Our derivation is more general since we do not assume the detailed modal field pattern in the resonator region.

approach in Eqs. (8)–(13). The maximum extinction ratio, defined as the power transmission ratio between the output port and the isolated port, reaches 45 dB. The extinction is limited by direct tunneling between the waveguides. The bandwidth for 30 dB isolation exceeds 6×10^{-5} (c/a).

The steady-state field patterns at a frequency $0.3468(c/a)$, where maximum isolation occurs, are shown in Fig. 7. In the absence of magneto-optical material in the cavity, light is transmitted to both output ports (Fig. 7a). In contrast, the magneto-optical resonator shows nearly 100% transmission to the output port and zero transmission to the isolated port (Fig. 4b). Moreover, light incident into the output port is completely dropped to the isolated port (Fig. 7c) and light incident into the isolated port is transferred to the input port (Fig. 7d). Evidently, an ideal isolator characteristics is observed at the operational frequency and the input port is therefore free from the back reflections from the output port.

The proposed device occupies only a small footprint of a few wavelength square. While the simulation in this paper is two-dimensional, the coupled-mode theory analysis, and hence the principles of the device, applies to three-dimensional cavity systems. For implementations in BIG thin films, the material exhibits strong gyrotropy with ε_a saturated at 0.06 [17, 18]. From the coupled-mode theory, the bandwidth of the circulator scales linearly with the magneto-optical coupling strength. Hence the ideal BIG device can provide a large bandwidth for 30 dB isolation up to 213 GHz, when operating at 633 nm. Since the quality factor of the resonator due to waveguide coupling can be as low as 140, the relative large material absorption in BIG can be still tolerated. At optical communication wavelength of 1550 nm, Ce:Yttrium Iron Garnet (Ce:YIG) has ε_a saturated at 0.009 with very low absorption [19]. For this material system, the bandwidth for 30 dB isolation at 1550 nm is estimated as 12.6 GHz.

6 Conclusions

In summary, we have demonstrated the magneto-coupling in two-dimensional photonic crystal defects can create extremely compact nonreciprocal modes. By coupling such nonreciprocal resonator to photonic crystal waveguides, we have designed a junction optical circulator with a 30 dB isolation bandwidth up to 213 GHz in BIG crystals. The strength of the magneto-coupling is optimized by maximizing the spatial overlap between the magnetization vector and the modal cross product.

A hybrid magneto-optical cavity in silicon/air photonic crystal also exhibits large magneto-coupling, while holding the advantage of better compatibility with existing planar integrated optical circuits. Also, by inverting the magnetization, complete transmission is switched from the output port to the isolated port. (This can be seen in Eq. (14), where inverting the magnetization results in the switch between ω_+ and ω_-.) Therefore, high-density non-volatile reprogrammable optical circuits may be implemented on existing silicon-based technology.

REFERENCES

1 A.K. Zvezdin, V.A. Kotov, *Modern Magnetooptics and Magnetooptical Materials* (Institute of Physics Pub., Bristol, Philadelphia, PA, 1997)
2 R. Wolfe, R.A. Lieberman, V.J. Fratello, R.E. Scotti, N. Kopylov, Appl. Phys. Lett. **56**, 426 (1990)
3 M. Levy, I. Ilic, R. Scarmozzino, R.M. Osgood, Jr., R. Wolfe, C.J. Gutierrez, G.A. Prinz, IEEE Photonics Technol. Lett. **5**, 198 (1993)
4 M. Levy, IEEE J. Sel. Top. Quant. **8**, 1300 (2002)
5 M. Inoue, K. Arai, T. Fujii, M. Abe, J. Appl. Phys. **83**, 6768 (1998)
6 M.J. Steel, M. Levy, R.M. Osgood, IEEE Photonics Technol. Lett. **12**, 1171 (2000)
7 Y. Xu, Y. Li, R.K. Lee, A. Yariv, Phys. Rev. E **62**, 7389 (2000)
8 S. Fan, P.R. Villeneuve, J.D. Joannopoulos, H.A. Haus, Phys. Rev. Lett. **80**, 960 (1998)
9 Z. Deng, E. Yenilmez, J. Leu, J.E. Hoffman, E.W.J. Straver, H. Dai, K.A. Moler, Appl. Phys. Lett. **85**, 6263 (2004)
10 H.A. Haus, *Waves and Fields in Optoelectronics* (Prentice-Hall, Englewood Cliffs, NJ, 1984)
11 S. Fan, W. Suh, J.D. Joannopoulos, J. Opt. Soc. Am. A **20**, 569 (2003)
12 W. Suh, Z. Wang, S. Fan, IEEE J. Quantum Electron. **40**, 1511 (2004)
13 J.D. Jackson, *Classical Electrodynamics* (Wiley, New York, 1999)
14 A.P. Zhao, J. Juntunen, A.V. Raisanen, IEEE Trans. Microwave Theory Tech. **47**, 1142 (1999)
15 M. Notomi, A. Shinya, E. Kuramochi, S. Mitsugi, H.Y. Ryu, *Slow-Light Waveguides and High-Q Nano-Resonators in Photonic Crystal Slabs*, presented at the OSA Annual Meeting (Rochester, NY, 2004)
16 A.G. Gurevich, G.A. Melkov, *Magnetization Oscillations and Waves* (CRC Press, Boca Raton, 1996)
17 T. Tepper, C.A. Ross, J. Cryst. Growth **255**, 324 (2003)
18 N. Adachi, V.P. Denysenkov, S.I. Khartsev, A.M. Grishin, T. Okuda, J. Appl. Phys. **88**, 2734 (2000)
19 M. Huang, S.Y. Zhang, Appl. Phys. A **A74**, 177 (2002)
20 S.G. Johnson, J.D. Joannopoulos, Optics Express **8**, 173 (2001)